# Correlated Visible-Light Absorption and Intrinsic Magnetism of SrTiO₃ Due to Oxygen Deficiency: Bulk or Surface Effect?

Heechae Choi,[†] Jin Dong Song,[‡] Kwang-Ryeol Lee,[†] and Seungchul Kim*,[†]

[†]Center for Computational Science and [‡]Center for Optoelectronics Convergence System, Korea Institute of Science and Technology, Hwarangro 14 Gil 5, 136-791, Seoul, Korea

Ⓢ Supporting Information
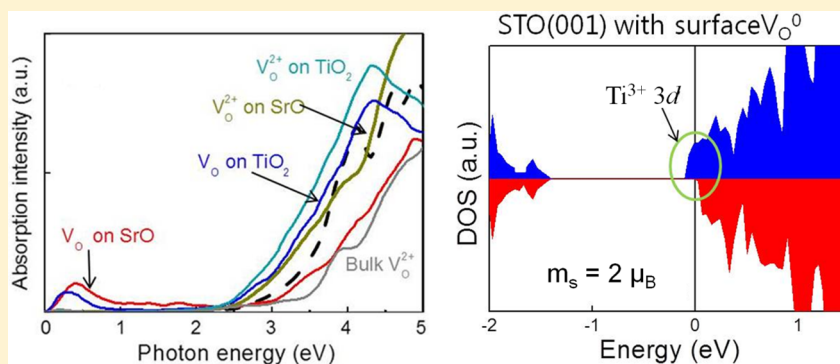
ABSTRACT: The visible-light absorption and luminescence of wide band gap (3.25 eV) strontium titanate (SrTiO₃) are well-known, in many cases, to originate from the existence of natural oxygen deficiency in the material. In this study based on density functional theory (DFT) calculations, we provide, to the best of our knowledge, the first report indicating that oxygen vacancies in the bulk and on the surfaces of SrTiO₃ (STO) play different roles in the optical and magnetic properties. We found that the doubly charged state of oxygen vacancy (V_O^{2+}) is dominant in bulk SrTiO₃ and does not contribute to the sub-band gap photoexcitation or intrinsic magnetism of STO. Neutral oxygen vacancies (V_O^0) on (001) surfaces terminated with both TiO₂ and SrO layers induce magnetic moments, which are dependent on the charged state of V_O. The calculated absorption spectra for the (001) surfaces exhibit mid-infrared absorption (<0.5 eV) and sub-band gap absorption (2.5−3.1 eV) due to oxygen vacancies. In particular, V_O^0 on the TiO₂-terminated surface has a relatively low formation energy and magnetic moments, which can explain the recently observed spin-dependent photon absorptions of STO in a magnetic circular dichroism measurement [Rice, W. D.; et al. *Nat. Mater.* **13**, 481, **2014**].

INTRODUCTION

Tuning the optical and magnetic properties of wide band gap oxides is of great scientific and technological interest and has driven robust efforts in defect engineering.[1−3] The defects of oxides can change the energy ranges of photoabsorption or emission and can induce intrinsic magnetism without doping.[2−4] The photon energies of absorption and emission are significantly influenced by the position of the defect levels, and the intensity of intrinsic magnetism of an undoped oxide is determined by the number of unpaired electron spins at the defect levels.[5−13] Therefore, defect-induced magnetic properties of an oxide can be directly correlated with the optical properties.

SrTiO₃ (STO) is one of the most intriguing optoelectronic materials with a wide band gap (3.25 eV).[14−18] The reported defect-induced sub-band gap absorption of undoped STO covers a wide range of photon energies, namely, ultraviolet (UV), green, blue, and, as an extraordinary case, mid-infrared (MIR).[17−19] The intrinsic nonstoichiometry of STO, dominated by oxygen deficiency (SrTiO₃₋δ), is known to be the main origin of the visible-light absorption and emission peaks.[18,19] Recently, magnetic circular dichroism (MCD) measurement by Rice et al. revealed that oxygen-deficient STO film exhibits spin-dependent photoexcitation, which implies the intrinsic magnetic moments of undoped STO.[18] The opto-magnetic excitations and corresponding optical "writing" in STO occur in the visible spectral range of 2.7−3.1 eV, which was attributed to the in-gap states induced by *bulk* oxygen deficiency, similar to Xie's earlier observation of 2.5−3.1 eV photon energy absorption in oxygen-deficient STO.[19] On the basis of the newly found fascinating capability of STO, optical writing of data is expected to enable the building of ultrafast nonvolatile memory devices[18−21] using visible light. However, the operation of the recently reported magnetic writing on STO was limited to very low temperatures (<10 K), possibly due to very weak exchange interaction between magnetic defects.[18]

In *bulk* STO (not on the surface), a doubly charged oxygen vacancy (V_O^{2+}) is compensated with two free electron carriers under ambient conditions. The experiments by Chan et al.[22] clearly demonstrated the dominance of V_O^{2+} in *bulk* STO, showing $-1/6$ slope of electron carrier concentrations (n) to log P_{O2}, where P_{O2} is the oxygen pressure, that is the result of the reaction

$$O_O^x \rightarrow V_O^{2+} + 2e^- + 1/2 O_{2(g)}$$
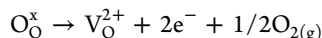
$$K = \frac{[V_O^{2+}]n^2 P_{O_2}^{1/2}}{[O_O^x]}$$

$$P_{O_2}^{-1/2} \propto [V_O^{2+}]n^2 = 2n^3$$

$$n \propto P_{O_2}^{-1/6}$$

The density functional theory (DFT) calculations done recently[23] also demonstrated the dominance of V_O^{2+} in bulk STO among all other point defects, even under oxygen-rich synthesis conditions.

However, much experimental evidence has implied that the *surface* oxygen vacancies on STO exist, and they might play more crucial roles in the visible-light absorptions than bulk defects do.[17,22,24] For example, the transmission electron microscopy (TEM) images of the blue-emitting Ar⁺-irradiated STO (001) thin film clearly shows highly reduced STO ($SrTiO_{3-\delta}$) layers near the surface layer coexists with bulk oxygen vacancies formed by irradiation.[22] Moreover, the oxygen vacancy segregation on grain boundaries was proven to be energetically stable in STO nanoparticles by Kim et al. with the electron energy-loss spectra.[17] In addition, the 470 nm photoluminescence (PL) peak was observed only in reduced nanocrystalline STO, which has large surface/volume ratio, while it was not in bulk STO under the same conditions.[25] This observation implies that PL at 470 nm is related to the surface.

Regarding the magnetic properties, it is doubtful that bulk V_O is the origin of intrinsic magnetism of undoped STO. The intrinsic magnetism of STO also may be originated from the surface vacancies because the V_O^{2+} in the bulk obviously induces zero spin moments as a result of the ground state of the neighboring Ti^{4+} ion being a singlet spin.[26] In *n*-type oxides, such as In_2O_3, SnO_2, and ZnO, unpaired electron spin(s) in the d- or f-orbital of the cation (metal ion) must have nonzero magnetic moments.[4,11,16,17,27] Hence, the d⁰-magnetism of *n*-type oxides might be primarily induced by the oxygen vacancies on surfaces[4,28] due to the lack of the crystal fields on the cation in the surface-normal direction. The possible origin of intrinsic magnetism of naturally grown *n*-type STO can be, therefore, unpaired 3d electron spins on the Ti ion near V_O. Hence, we raised the possibility of the different roles of the oxygen deficiencies of surface and bulk STO.

Because the experimental measurements on the photo-luminescence and magnetization of oxides provided mixed signals from the bulk and surface regions, it is necessary to separately understand the roles of oxygen deficiency on the STO surface and in bulk to precisely control the magnetic and optical properties.

Motivated by determining how the surface and bulk oxygen vacancies of STO behave differently, we investigated the effects of oxygen vacancies on the optical and magnetic properties of STO using first-principles calculations. We considered both the bulk and the surface of STO and included the charge state

variation on the oxygen vacancy. For the surface model of STO, we considered the most frequently observed STO (001) surface orientations.[29,30]

■ CALCULATION METHODS

We used periodic supercell model structures of $4 \times 4 \times 4$ unit cells for the bulk and symmetric $4 \times 4 \times 3$ slabs for the surfaces, as displayed in Figure 1. Slabs in adjacent supercells are separated with 12.0 Å of
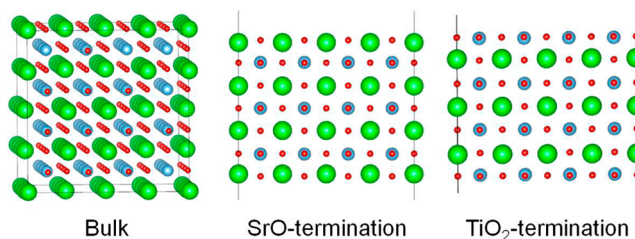
Figure 1. Supercells of $SrTiO_3$ (STO) bulk and surfaces, of which the sizes are $4 \times 4 \times 4$ and $4 \times 4 \times 3$, respectively. The green, blue, and red spheres indicate Sr, Ti, and O atoms, respectively.

vacuum. The size of the supercell was chosen following the suggestions from the careful convergence test of the previous DFT works.[23,31] One oxygen atom was taken away to generate an oxygen vacancy in the bulk or on the surfaces. The convergence test for bulk system by Ertekin[23] revealed that defect−defect interaction energy converges far below 0.01 Ry when the cell size is $4 \times 4 \times 4$; hence, this size is proper for the modeling of dilute point defects in bulk system. Carrasco et al. conducted the convergence test for surface system,[31] where $4 \times 4 \times 3$ slab with 240 atoms was found to give reliable vacancy formation energy with only 0.7 and 0.6% of energy deviations from $3 \times 3 \times 5$ and $3\sqrt{2} \times 3\sqrt{2} \times 3\sqrt{2}$ slabs with 225 and 270 atoms, respectively.

We performed DFT total energy calculations[32] within the generalized gradient approximation (GGA) using Perdew−Burke−Ernzerhof (PBE) parametrization.[33,34] We used VASP software,[32] and the atomic nuclei and core electrons were described by a projector-augmented wave (PAW).[35−37] Khon−Sham orbitals were expanded with a cutoff energy of 400 eV. Equally spaced *k*-point grids of $3 \times 3 \times 3$ and $3 \times 3 \times 1$ were used for the Brillouin zone sampling in the $4 \times 4 \times 4$ bulk cell and the $4 \times 4 \times 3$ slab cell.[38] A Hubbard U parameter[39] of Ti ($U_{3d} = 3$ eV) included electronic structure calculations to correct the underestimated band gap in PBE calculations and to improve absorption spectra calculations. In our PBE and PBE+U calculations, the theoretical band gaps were 1.89 and 2.40 eV, respectively.

The formation energy (ΔE^f) of the oxygen vacancy (V_O) was calculated with a varying charge q using the equation[40]

$$\Delta E^f(q) = E[V_O^q] + \mu_O - E^0 + q(E_v + \Delta V + E_F) \quad (1)$$

where $E[V_O^q]$ is the total energy of the V_O-containing STO supercell with a charge q, E^0 is the total energy of the defect-free STO, μ_O is the chemical potential of oxygen removed from the STO, E_v is the valence band maximum (VBM) of the defect-free STO, ΔV is the shift in the VBM in the defective cell by a point defect relative to that in the defect-free STO, and E_F is the Fermi level referenced to E_v. The chemical potential of oxygen was calculated using the thermodynamic equation for ideal gases and the chemical potential at standard temperature and pressure. The oxygen chemical potential was expressed as

$$\mu_O(T, P_{O_2}) = \frac{1}{2}\left\{\tilde{\mu}_{O_2}(T, P_{O_2}^0) + k_B T \ln\left(\frac{P_{O_2}}{P_{O_2}^0}\right)\right\} \quad (2)$$

where $\tilde{\mu}_{O_2}(T, P_{O_2}^0)$ is the O_2 chemical potential at standard pressure ($P_{O_2}^0 = 0.2$ atm) and the given temperature T.[41] The experimental binding energy of an oxygen molecule, 2.56 eV/atom,[42] was used instead of the GGA value to avoid the well-known overestimating error

of GGA calculations on oxygen double bond (O═O) strength. By taking the experimental value of the O═O binding energy, we obtained the theoretical formation energy of STO = −16.78 eV/f.u., which is even closer to the experimental value of −17.13 eV/f.u.[43] than the computed value using hybrid functional method, −16.22 eV/f.u.[44]

Since Hubbard U does not fully correct band gap, the transition point of defect charge was further corrected by extrapolating its change from PBE to PBE+U using the following equation.[45,46]

$$\epsilon(q/q') = \epsilon(q/q')^{PBE+U} + \frac{\Delta\epsilon}{\Delta E}(E_g^{exp} - E_g^{PBE+U}) \quad (3)$$

with

$$\frac{\Delta\epsilon}{\Delta E} = \left(\frac{\epsilon(q/q')^{PBE+U} - \epsilon(q/q')^{PBE}}{E_g^{PBE+U} - E_g^{PBE}}\right) \quad (4)$$

where $\epsilon(q/q')$ is the transition point from charge q to q'. E_g^{exp}, E_g^{PBE+U}, and E_g^{PBE} are the band gap energy obtained from experiments, PBE+U, and PBE, respectively. The coefficient $\Delta\epsilon/\Delta E_g$ is the rate of charge transition level change with respect to the change of band gap.

The photoabsorption coefficient (α) was calculated using the following equations.

$$\alpha(\lambda) = 4\pi\kappa/\lambda$$

$$\kappa = ((\epsilon_1^2 + \epsilon_2^2)^{1/2} - \epsilon_1)/2)^{1/2} \quad (5)$$

where ε_1 and ε_2 are the real and imaginary parts, respectively, of the complex dielectric constant, $\varepsilon = \varepsilon_1 + i\varepsilon_2$. In general, the theoretical dielectric constants obtained using the GGA or local density approximation (LDA) methods exhibit noticeable mismatches, both in phase and in magnitude.[47,48] When the Hubbard's U term is included, the DFT calculations on the complex dielectric constants of metal oxides are strikingly improved by weakening the serious self-interaction errors of the GGA or the LDA.[49] Our PBE+U calculations of the dielectric constant of STO systems also well-matched both the real and imaginary parts up to 6 eV, which covers our region of interest (see Figure S1 of Supporting Information).

■ RESULTS AND DISCUSSION

A. Formation of O-Deficiency and Its Effects on the Magnetic Properties. In Table I, the formation energies at standard conditions (T = 298 K, P_{O2} = 0.2 atm; ΔE_{std}^f) and the resultant magnetic moments are presented. In particular, ΔE^f has a negative value on the TiO$_2$-terminated surface, which is consistent with the recent experimental result.[50] As summarized in Table I, the magnetic moments induced by V$_O$ are dependent on the charged state of V$_O$. The bulk magnetism

Table I. Calculated ΔE_{std}^f of V$_O$ at Standard Temperature and Pressure and the Induced Magnetic Moments for Varying Charge States

system	V$_O$ charge	ΔE_{std}^f E_F = VBM	ΔE_{std}^f E_F = CBM	magnetic moment (μ_B)
bulk	0	5.30	5.30	1.0
	1+	0.59	3.84	0.0
	2+	−2.02	4.48	0.0
TiO$_2$-terminated surface	0	1.43	1.43	2.0
	1+	0.82	4.07	1.0
	2+	0.35	6.85	0.0
SrO-terminated surface	0	2.54	2.54	2.0
	1+	1.64	4.89	1.0
	2+	1.21	7.71	0.0

arises only from the neutral vacancy with a magnitude of 1.0 μ_B, while the surface oxygen vacancies have magnitudes of 2.0, 1.0, and 0.0 μ_B for the neutral, single, and double charge states, respectively.

In Figure 2, the calculated ΔE_{std}^f values are plotted. The correction of the charge transition point of bulk V$_O$ using eq 3
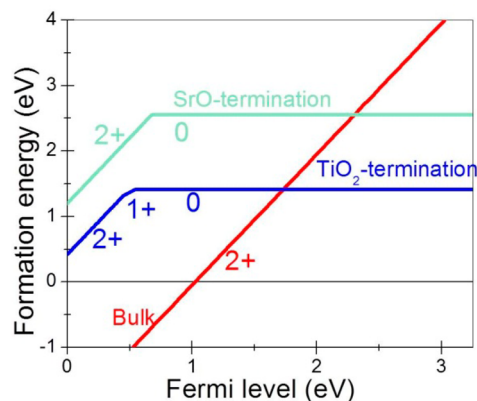
Figure 2. ΔE_{std}^f of V$_O$ with different charged states in bulk and on surfaces as a function of the Fermi level. E_F changes from the VBM (0 eV) to the CBM (3.25 eV).

makes our DFT+U calculation results well-consistent with the hybrid functional method.[45] Doubly charged V$_O$ in bulk is dominant when the Fermi level is close to the VBM (p-type), and neutral V$_O$ on the TiO$_2$-terminated surface is dominant when the Fermi level is close to the conduction band minimum (CBM) (n-type). The V$_O$ in STO bulk always prefers the doubly charged state (V$_O^{2+}$) for a value of the Fermi level (E_F) throughout the entire band gap due to its low formation energy. Therefore, oxygen deficiency in the bulk of STO is not responsible for the intrinsic d^0-magnetism of STO due to the lack of magnetic moments (Table I). In contrast, V$_O$ on the (001) surface for both TiO$_2$- and SrO-termination is primarily in the neutral charge state. When the TiO$_{2-x}$ layer appears on the surfaces, a magnetic moment of 2.0 μ_B is induced per V$_O$. In an as-prepared natural STO film, the (001)-oriented surface is dominant and is primarily terminated with a TiO$_{2-x}$ layer.[29,30] Therefore, we strongly expect that the intrinsic magnetism of STO (001) in the oxygen-deficient condition[16] primarily originates from the neutral oxygen vacancy on the TiO$_2$-terminated surface.

In some special environments, for example, H$_2$O-rich condition or HF etching, the termination of an STO (001) turns to a SrO-layer, despite its larger surface tension than that of the TiO$_2$-layer.[29,30] Because of the larger formation energy of V$_O^0$ on the surface with SrO-termination than that on the surface with TiO$_2$-termination, the magnetization intensity of the STO (001) system is expected to be decreased when the SrO-layer is at the surface. Hence, the magnetic properties of STO nanostructures are controllable via the surface termination.

Fully relaxed structures exhibit significant changes of the bonding lengths, such that the Ti−O bond lengths nearest the V$_O$ site are 4.2% and 15.1% increased when the charge of oxygen vacancy on TiO$_2$-termination is changed from V$_O^{2+}$ to V$_O^{1+}$ and V$_O^0$, respectively (Figure 3). Generally, large lattice relaxation via charge transition causes large deviations of the emission photon energy from the absorption photon energy.[51]
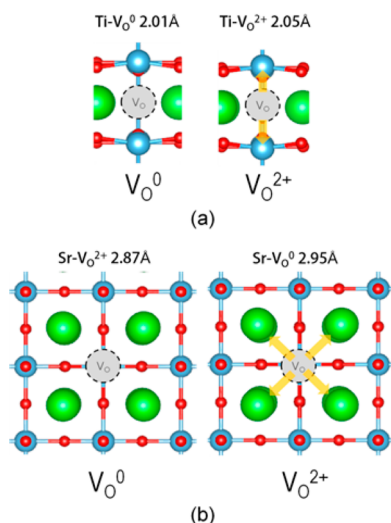
Figure 3. Atomic structures (top view) near V_O^0 and V_O^{2+} on (a) TiO_2- and (b) SrO-terminated STO (001) surfaces. Significant lattice relaxation occurs on both surfaces via the charge transitions of V_O.

Ti ions at the vicinity of neutral and singly charged V_O have unpaired 3d electrons, which induce magnetic moments, while a doubly charged V_O does not induce a magnetic moment (Table I and Figure 4). Because an oxygen vacancy in the bulk
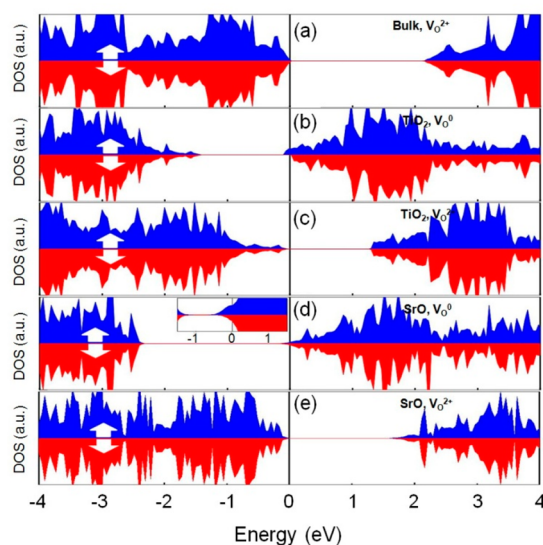

Figure 4. Electron DOS. (a) V_O^{2+} in STO bulk. (b) V_O^0 and (c) V_O^{2+} on the TiO_2-terminated surface. (d) V_O^0 and (e) V_O^{2+} on the SrO-terminated surface. Magnified inset in (d) shows the different DOS of spin up and spin down around the Fermi level. The highest occupied state was set to be zero energy.

always prefers the doubly charged state (V_O^{2+}), the bulk oxygen vacancies cannot induce magnetic moments at all (Figure 4a), which is different from the suggestions of several reports.[5,11−16] However, partially "reduced" vacancies at the surfaces induce magnetic moments (Figure 4b,d and Table I). This result strongly implies that the *observed magnetism of STO at oxygen-deficient condition originates from oxygen vacancies on the surfaces and not from those in the bulk.*

When V_O is doubly charged, the valence states of STO bulk and surface states or defect states near the VBM are fully occupied (Figure 4a,c,d) because all ions in the system are fully

oxidized (for metal ions) or reduced (for oxygen ions). V_O and V_O^+ at both SrO- and TiO_2-terminated surfaces induce unpaired 3d states just below the CBM of STO bulk, giving 2.0 and 1.0 μ_B, respectively, to the system. For the TiO_2-terminated surface, two surface Ti^{3+} ions adjacent to V_O^0 have 2.0 μ_B of magnetic moment in total, 1.0 μ_B per Ti^{3+} ion (Figure 5a). For the SrO-terminated surface, one Ti atom at the
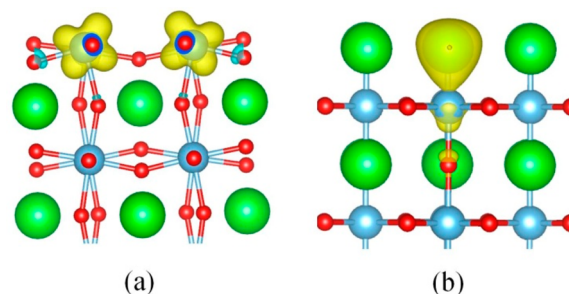
Figure 5. Spin density plots of STO surfaces with V_O^0 on (a) TiO_2- and (b) SrO- terminated surfaces (side-view). Green, blue, and red spheres indicate Sr, Ti, and O atoms, respectively. The isovalue is 0.005 $\mu_B/Å^3$.

subsurface has 2.0 μ_B (Figure 5b). Interestingly, V_O^0 at the surface of TiO_2 termination produces fully spin-polarized states (Figure 4b). V_O^0 at the surface of SrO termination also induces magnetic moments to the surface, but its spin is not fully polarized (Figure 4d). Because the surface of TiO_2 termination is dominant, we suggest that V_O^0 on the surface of TiO_2 termination is responsible for the recently observed spin-dependent optical absorption in the 2.7 to 3.1 eV spectral range in oxygen-deficient STO (001).[18]

Next, we examined the magnetic ordering of V_O TiO_2-terminated surface only due to the energetic preference of TiO_2-termination. Energies of various positions of V_O and spin configurations were calculated, as Figures 6 and 7 show. We tested exchange energies perpendicular and parallel to the $Ti^{3+}-V_O^0-Ti^{3+}$ chains, as shown in Figure 6a,b, separately using 4×2 and 2×4 cells. The energy differences are presented in Table II.

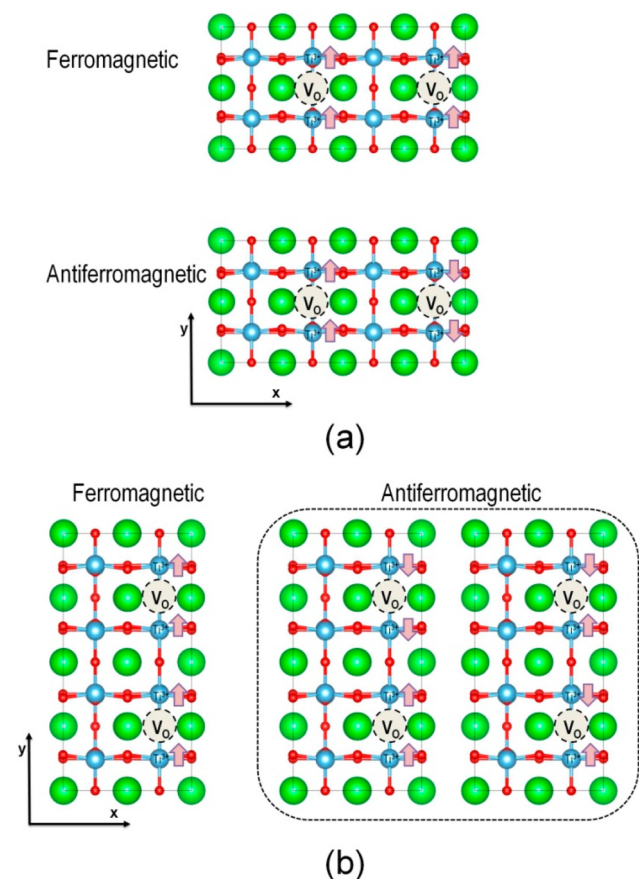**Table II. Magnetic Moments and Relative Total Energies (ΔE) with Varying Spin Orderings**

interaction direction[a]	spin ordering	magnetic moment (μ_B)	ΔE (meV)
x-direction	↑-↑-↑-↑	4.0	0
	↑-↑-↓-↓	0.0	+3
y-direction	↑-↑-↑-↑	4.0	0
	↑-↓-↑-↓	0.0	−20
	↑-↑-↓-↓	0.0	−14

[a]The x- and y-direction indicates structures in Figure 6a,b, respectively.

Energetics implies that alternating ordering of spin is preferred, and superexchange interaction is the main mechanism of magnetic ordering. Additionally, spins on two Ti^{3+} next to the same V_O align in the same direction. In Figure 6b, ferromagnetic ordering is higher in energy than antiferromagnetic ordering because superexchange interaction mediated by O 2p induces opposite direction of spin in $Ti^{3+}-O-Ti^{3+}$, where two Ti ions are the neighbors of different V_O. In the structure of Figure 6a, two Ti^{3+} ions are connected in the way of $Ti^{3+}-$
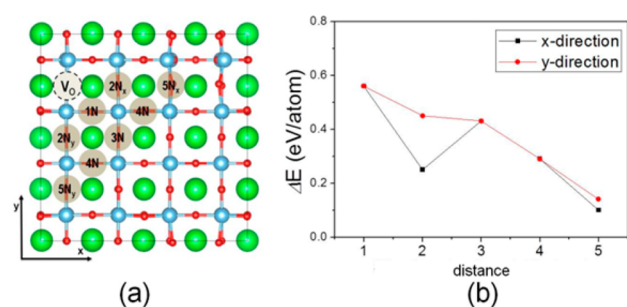
$O-Ti^{4+}-O-Ti^{3+}$, and, by the two times of superexchange interaction, spins align in the same direction.

The exchange energy decreases rapidly; it becomes in the order of millielectronvolts for ~8 Å of inter V_O distance (Figure 6a). V_Os tend to distribute dispersively, as energy gradually decreases when V_Os are gradually away from each other (Figure 7). Along with very small exchange energy, STO surface is expected to be paramagnetic under moderate condition. Magnetic ordering requires specific ordering of V_Os although it needs not to be the periodic reconstruction, and the necessary (but not sufficient) conditions are highly oxygen-deficient and cryogenic environment.

Figure 7. (a) Top view of 4 × 4 TiO_2-terminated STO(001) surface with the marked position of the existing V_O (marked with dotted circle) and positions of second V_O, and (b) relative formation energies (ΔE) of two V_O, compared to that of single V_O (referenced as zero). V_Os at 2nd and 5th neighbor sites in x- and y-direction are inequivalent, while others are equivalent.

Figure 6. Surface models of STO with (a) 4 × 2 and (b) 2 × 4 cells with two V_O^0 aligning in x- and y-directions, respectively. For the y-direction alignments of V_O^0, two different antiferromagnetic ordering was considered: ↑-↑-↓-↓ (left) and ↑-↓-↑-↓ (right).

B. Optical Absorption Characteristics of O-Deficient Bulk STO and STO (001) Surfaces. The wide band gap (3.25 eV) and the intrinsic magnetism due to impurity bands can make STO applicable in opto-magnetic devices in the visible light range, as already demonstrated in the MCD measurements in the literature.[18] Therefore, the predictions on the absorption spectra due to defects of varying charge state are useful to prepare light-emitting diodes[19,24] or optically writable oxides via d^0-magnetism for certain wavelengths of light.[16] We present the calculated absorption spectra of bulk and slab STO with and without oxygen vacancies (Figure 8). In Figure 8a, we present defect-free bulk and (001) surfaces to illustrate the effects of termination on the optical absorptions. The absorption peaks at 4 and 5 eV of defect-free bulk STO are

well-matched with the experimental measurements,[14,−22,52−54] which support the reliability of our calculations. Especially, the hypothesis that surface oxygen vacancy is the origin of having stronger PL peaks at 470 nm for nanoparticle, rather than bulk STO, can be supported by our results. The direct comparison between the experimental and theoretical absorption spectra is given in Figure S2 of Supporting Information.

We observed two distinguishing features of defective surfaces from the bulk: absorption in the MIR range (<0.5 eV) and at sub-band gap ($\lesssim$ 3.2 eV), as presented in Figure 8b. The enhanced visible light-absorption at 2.4 to 3.2 eV range are magnified in Figure 8c for convenience. Absorption in the MIR range has been observed only in a heavily reduced STO sample at high temperature,[52] which agrees well with our calculations. Hence, to achieve a MIR absorber with STO, the surface must be reduced to generate oxygen vacancies, and the sample should not be p-type, to ensure that V_O is neutral.

Defect-free STO (001) surfaces with both terminations exhibit no absorption in the sub-band gap range (Figure 8a). In Figure 8b, however, we find absorption in the sub-band gap range of 2.7 to 3.1 eV for both V_O^0 and V_O^{2+} at the surfaces. This observation is consistent with the report by Rice et al.[18] and Xie et al.[19] that the optical absorption occurs at the midgap bands of oxygen-deficient STO. Indeed, we strongly infer that oxygen vacancies on the surface of TiO_2 termination are the source of magnetization reversal by photoexcitations with circularly polarized light in the 2.7−3.1 eV range in the experiment[18,19] rather than those on the surfaces of SrO termination due to the low surface energy of the TiO_2-terminations, the low formation energy of V_O, and the magnetically polarized V_O^0 on the TiO_2-terminated surface. Therefore, we propose that STO structures should be tailored to have a high surface/volume ratio for magneto-optic applications.

We calculate projected density of states (PDOS) and joint density of states (JDOS) to investigate the optical absorptions of STO (Figure 9). In accordance to the energetic stability, we calculated V_O on the TiO_2-terminated surface. The JDOS is obtained using eq 6.

$$JDOS_{\alpha\beta}(\varepsilon) = \int_{E_F}^{\infty} D_o^\alpha(E - \varepsilon) D_u^\beta(E) dE \tag{6}$$

where $D_O^\alpha(E)$ and $D_u^\beta(E)$ are occupied and unoccupied electronic DOS of atom α and β. Hence, JDOS provides possible electron transition from atom α to β by the photon energy ε. Note that JDOS is not the transition probability itself.
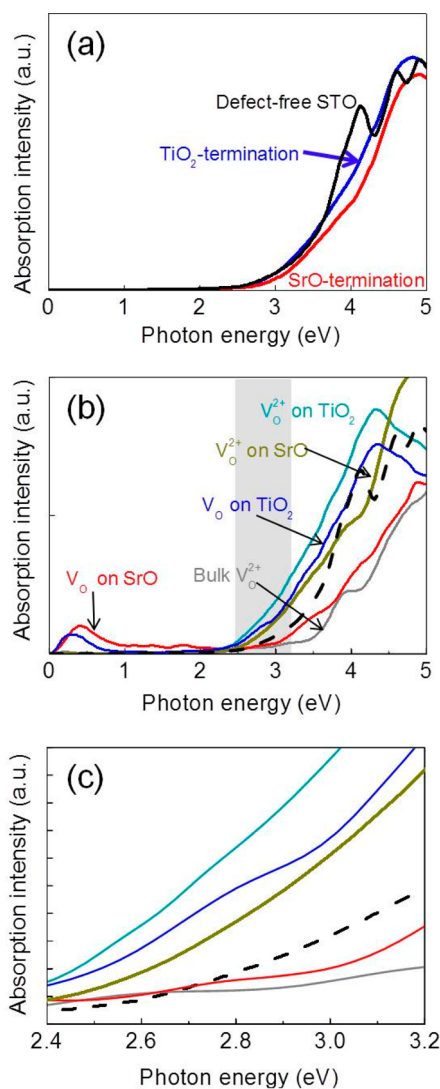
Figure 8. Calculated optical absorption spectra of (a) defect-free STO surfaces and bulk and (b, c) O-deficient STO surfaces and bulk. For comparison, the black dashed line for the defect-free STO bulk is inserted in (b, c). The graph in (c) is the magnified one of (b) for the photon energy range of the shaded area.

We consider the transition between O 2p and Ti 3d around the V_O, and ignore O 2p $\rightarrow$ 2p and Ti 3d $\rightarrow$ 3d transition as being due to the selection rule ($\Delta l = \pm 1$). Figure 9a presents PDOS of surface Ti^{3+}, which is adjacent to V_O^0, O^{2-} underneath Ti^{3+} (O_{under}), and the corresponding JDOS is presented in Figure 9b. PDOSs of other oxygen atoms were not drawn as their PDOSs near the band edges are very small. Ti^{3+} d orbital around the E_F consists of d_{yz}, d_{z^2}, and d_{xz} (Figure 9c), so it is the combination of $^2D_{\pm 3/2}$ and $^2D_{\pm 1/2}$.

Optical absorption at MIR and sub-band gap might be the result of transition between 3d of Ti^{3+} and 2p of O_{under}. Ti atoms next to V_O are under-coordinated and have one 3d electron that is located just below CBM of STO bulk (Figure 9a). Absorption at ~0.2 eV in Figure 8b occurs by the transition from occupied Ti^{3+} 3d states to unoccupied O_{under} 2p. Sub-band gap absorption occurs by the transition from O_{under} $2p_z$ above the bulk VBM ($E < -1.5$ eV in Figure 9c) to Ti^{3+} 3d. As discussed, the surface is paramagnetic. However, magnetic polarization of Ti^{3+} 3d will lead polarization-
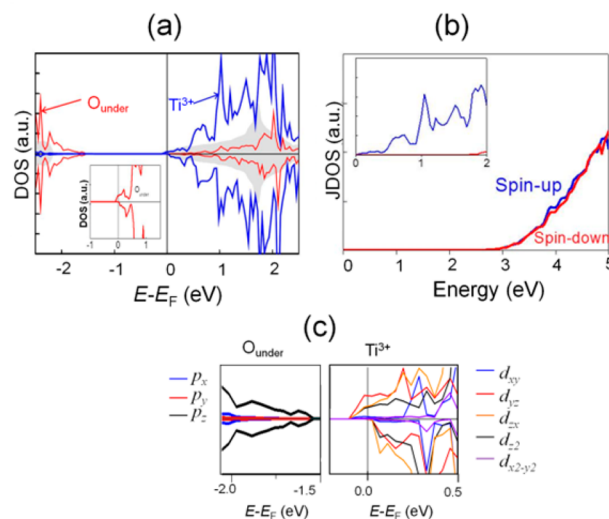
Figure 9. (a) The PDOS of surface Ti^{3+} 3d-orbital (blue) and O^{2-} 2p-orbital (red) underneath the Ti^{3+}. The gray shade is the DOS of defectless bulk STO. (b) The calculated JDOS of O_{under} and Ti^{3+}, and (c) PDOS around E_F and VBM. The inset in (b) is magnified JDOS plots.

dependent optical absorption under applied magnetic field, such as MCD measurement condition.

■ CONCLUSION

We demonstrated that oxygen vacancies on STO (001) surfaces induce the intrinsic magnetization and that the charge state of oxygen vacancies determines the value of the magnetic moments. Contrary to the conventional belief, bulk oxygen deficiency does not induce a magnetic moment in the STO system because the doubly charged state (V_O^{2+}) removes the two unpaired 3d-orbital electron spins from the neighboring Ti atoms. From our findings, the dependence of magnetism on the surface termination of STO (001), and the charge state of the oxygen vacancy, we suggest that the magnetic properties of STO be tuned with the preparation of surface in the (001) direction or via electrical methods, such as gate voltages. Because the magnetic moments induced from TiO_2- and SrO-terminated surfaces exhibit the same dependency on the charge state of V_O, that is, they decrease with increasing charge, the oxygen vacancy at STO surfaces in other crystallographic directions may have similar magnetic properties. Finally, we propose that well-designed structures of STO with a large surface/volume ratio can be utilized for magneto-optical applications.

■ ASSOCIATED CONTENT

ⓢ Supporting Information

Comparisons of theoretical and experimental dielectric constants and absorption spectra of $SrTiO_3$. This material is available free of charge via the Internet at http://pubs.acs.org.

■ AUTHOR INFORMATION

Corresponding Author

*E-mail: sckim@kist.re.kr.

Notes

The authors declare no competing financial interest.

ACKNOWLEDGMENTS

REFERENCES

(1) Koehl, W. F.; Buckley, B. B.; Heremans, F. J.; Calusine, G.; Awschalom, D. D. *Nature* **2011**, *479*, 83.

(2) Chambers, S. *Nat. Mater.* **2010**, *9*, 956.

(3) Yi, J. B.; et al. *Phys. Rev. Lett.* **2010**, *104*, 137201.

(4) Ogale, S. B. *Adv. Mater.* **2010**, *22*, 1915.

(5) Choi, H.; Cho, S. H.; Khan, S.; Lee, K.-R.; kim, S. *J. Mater. Chem. C* **2014**, *2*, 6017.

(6) Choi, H.; Lee, E.-K.; Cho, S. B.; Yoo, D. S.; Chung, Y.-C. *IEEE Electron Device Lett.* **2011**, *32*, 1287.

(7) Philip, J.; et al. *Nat. Mater.* **2006**, *5*, 298.

(8) Meng, X.; Tang, L.; Li, J. *J. Phys. Chem. C* **2010**, *114*, 17569.

(9) Peleckis, G.; Wang, X.; Dou, S. X. *Appl. Phys. Lett.* **2006**, *89*, 022501.

(10) Wang, V.; You, C.-Y.; He, H.-P.; Ma, D.-M.; Mizuseki, H.; Kawazoe, Y. *J. Magn. Magn. Mater.* **2013**, *348*, 55.

(11) Sundaresan, A.; Bhargavi, R.; Rangarajan, N.; Siddesh, U.; Rao, C. N. R. *Phys. Rev. B* **2006**, *74*, 161306(R).

(12) Zhu, Q.; Peng, Y.; Lin, L.; Fan, C.-M.; Gao, G.-Q.; Wang, R.-X.; Xu, A.-W. *J. Mater. Chem. A* **2014**, *2*, 4429.

(13) Fan, C.-M.; Peng, Y.; Zhu, Q.; Lin, L.; Wang, R.-X.; Xu, A.-X. *J. Phys. Chem. C* **2013**, *117*, 24157.

(14) Kim, H. W.; Na, H. G.; Kwak, D. S.; Kwon, Y. J.; Khai, T. V.; Lee, C.; Jung, J. H. *Thin Solid Films* **2013**, *546*, 219.

(15) Sudakar, C.; Dixit, A.; Kumar, S.; Sahana, M. B.; Lawes, G.; Naik, R.; Naik, V. M. *Scr. Mater.* **2010**, *62*, 63.

(16) Sun, S.; Wu, P.; Xing, P. *Appl. Phys. Lett.* **2012**, *101*, 132417.

(17) Kim, M.; Duscher, G.; Browning, N.; Sohlberg, K.; Pantelides, S. T.; Pennycook, S. J. *Phys. Rev. Lett.* **2001**, *86*, 4056.

(18) Rice, W. D.; et al. *Nat. Mater.* **2014**, *13*, 481.

(19) Xie, K.; Umezawa, N.; Zhang, N.; Reunchan, P.; Zhang, Y.; Ye, J. *Energy Environ. Sci.* **2011**, *4*, 4211.

(20) Kimel, A. V.; Kirilyuk, A.; Usachev, P. A.; Pisarev, R. V.; Balbashov, A. M.; Rasing, Th. *Nature* **2005**, *435*, 655.

(21) Stanciu, C. D.; Hansteen, F.; Kimel, A. V.; Kirilyuk, A.; Tsukamoto, A.; Itoh, A.; Rasing, Th. *Phys. Rev. Lett.* **2007**, *99*, 047601.

(22) Chan, N.-H.; Sharma, R. K.; Smyth, D. M. *J. Electrochem. Soc.* **1981**, *128*, 1762.

(23) Ertekin, E.; Srinivasan, V.; Ravichandran, J.; Rossen, P. B.; Siemons, W.; Majumdar, A.; Ramesh, R.; Grossman, J. C. *Phys. Rev. B* **2012**, *85*, 195460.

(24) Kan, D.; Terashima, T.; Kanda, R.; Masuno, A.; Tanaka, K.; Chu, S.; Kan, H.; Ishizumi, A.; Kanemitsu, Y.; Shimakawa, Y.; Takano, M. *Nat. Mater.* **2005**, *4*, 816.

(25) Zhang, W. F.; Yin, Z.; Zhang, M. S.; Du, Z. L.; Chen, W. C. *J. Phys.: Condens. Matter* **1999**, *11*, 5655.

(26) Lin, C.; Demkov, A. A. *Phys. Rev. Lett.* **2013**, *111*, 217601.

(27) Xiao, Z. R.; Fan, X. F.; Guan, L. X.; Huan, C. H. A.; Kuo, J. L.; Wang, L. *J. Phys.: Condens. Matter* **2009**, *21*, 272202.

(28) Dutta, P.; Seehra, M. S.; Zhang, Y.; Wender, I. *J. Appl. Phys.* **2008**, *103*, 07D104.

(29) Bachelet, R.; Sánchez, F.; Palomares, F.; Ocal, C.; Fontcuberta, J. *Appl. Phys. Lett.* **2009**, *95*, 141915.

(30) Radovic, M.; et al. *Appl. Phys. Lett.* **2009**, *94*, 022901.

(31) Carrasco, J.; Illas, F.; Lopez, N.; Kotomin, E. A.; Zhukovskii, Yu. F.; Evarestov, R. A.; Mastrikov, Yu. A.; Piskunov, S.; Maier, J. *Phys. Rev. B* **2006**, *73*, 064106.

(32) Ihm, J.; Zunger, A.; Cohen, M. L. *J. Phys. C* **1979**, *12*, 4409.

(33) Kohn, W.; Sham, L. J. *Phys. Rev.* **1965**, *140*, A1133.

(34) Perdew, J. P.; Burke, K.; Ernzerhof, M. *Phys. Rev. Lett.* **1997**, *77*, 3865.

(35) Perdew, J. P.; Burke, K.; Ernzerhof, M. *Phys. Rev. Lett.* **1997**, *78*, 1396.

(36) Kresse, G.; Hafner, J. *Phys. Rev. B* **1993**, *47*, 558.

(37) Perdew, J. P.; Chevary, J. A.; Vosko, S. H.; Jackson, K. A.; Pederson, M. R.; Singh, D. J.; Fiolhais, C. *Phys. Rev. B* **1992**, *46*, 6671.

(38) Monkhorst, H. J.; Pack, J. D. *Phys. Rev. B* **1976**, *13*, 5188.

(39) Dudarev, S. L.; Botton, G. A.; Savrasov, S. Y.; Humphreys, C. J.; Sutton, A. P. *Phys. Rev. B* **1988**, *57*, 1505.

(40) Van de Walle, C. G.; Neugebauer, J. *J. Appl. Phys.* **2005**, *95*, 3851.

(41) Stull, D. R.; Prophet, H. *JANAF Thermochemical Tables;* 2nd ed.; National Bureau of Standards, Washington, DC, 1971.

(42) Peressi, M.; Binggeli, N.; Balderreschi, A. *J. Phys. D* **1998**, *31*, 1273.

(43) Jacob, K. T.; Rajita, G. *J. Chem. Thermodyn.* **2011**, *43*, 51.

(44) Varley, J. B.; Janotti, A.; Van de Walle, C. G. *Phys. Rev. B* **2014**, *89*, 075202.

(45) Ferysoldt, C.; Grabowski, B.; Hickel, T.; Neugebauer, J.; Kresse, G.; Janotti, A.; Van de Walle, C. G. *Rev. Mod. Phys.* **2014**, *86*, 253.

(46) Janotti, A.; Van de Walle, C. G. *Phys. Rev. B* **2007**, *76*, 165202.

(47) Saha, S.; Sinha, T. P.; Mookerjee, A. *J. Phys. D* **1998**, *31*, 1273.

(48) Zollner, S.; Demkov, A. A.; Liu, R.; Fejes, P. L.; Gregory, R. B.; Curless, J. A.; Yu, Z.; Ramadani, J.; Droopad, R.; Tiwald, T. E.; Hilfiker, J. N.; Woollam, J. A. *J. Vac. Sci. Technol., B* **2000**, *18*, 2242.

(49) Ye, L.-H.; Luo, N.; Peng, L. M.; Weinert, M.; Freeman, A. J. *Phys. Rev. B* **2013**, *87*, 075115.

(50) Janotti, A.; Varley, J. B.; Choi, M.; Van de Walle, C. G. *Phys. Rev. B* **2014**, *90*, 085202.

(51) Zhang, J.; Doutt, D.; Merz, T.; Chakhalian, J.; Kareev, M.; Liu, J.; Brillson, L. J. *Appl. Phys. Lett.* **2009**, *94*, 092904.

(52) Crandles, D. A.; Nicholas, B.; Dreher, C.; Homes, C. C.; McConnell, A. W.; Clayman, B. P.; Gong, W. H.; Greedan, J. E. *Phys. Rev. B* **1999**, *59*, 12842.

(53) Bauerle, D.; Braun, W.; Saile, V.; Sprussel, G.; Koch, E. E. *Z. Phys. B* **1978**, *29*, 179.

(54) Yu, H.; Ouyang, S.; Yan, S.; Li, Z.; Yu, T.; Zou, Z. *J. Mater. Chem.* **2011**, *21*, 11347.